Journal of Materials Physics and Chemistry, 2013, Vol. 1, No. 4, 65-68
Available online at http://pubs.sciepub.com/jmpc/1/4/2

DOI:10.12691/jmpc-1-4-2

Microstructural Transformations of Dissimilar Austenite-Ferrite Stainless Steels Welded Joints

Sara Aguilar*, Ramón Tabares, Claudia Serna

Materials Engineering Department, University of Antioquia, Pyrometallurgical and Materials Research Group GIPIMME, Medellín, Colombia
*Corresponding author: saritamaria272@gmail.com

Received October 25, 2013; Revised November 12, 2013; Accepted November 14, 2013

Abstract This research studies the metallurgical transformations happening during the SMAW welding of AISI 316L austenitic stainless steel with AISI 430 ferritic stainless steel. Two different electrodes, AWS E309L austenitic and AWS E2209-16 duplex stainless steels 3.2 mm diameter, were used to perform the study. The joining was made with a single pass welding and keeping a low heat input ranging from 700 - 1000 J/mm. The influence of the type of electrode and the heat input on the microstructural evolution of the heat affected and the fusion zone was evaluated. Differences between δ ferrite morphology were found for both weld metals. The heat affected zone of the ferritic side showed grain coarsening and grain refinement with martensite at the grain boundaries. Tensile strength was similar for both welding conditions. Microhardness and δ ferrite percent were measured as well.

Keywords: *stainless steels welding, SMAW, welding metallurgy, austenitic stainless steel, ferritic stainless steel*

Cite This Article: Sara Aguilar, Ramón Tabares, and Claudia Serna, "Microstructural Transformations of Dissimilar Austenite-Ferrite Stainless Steels Welded Joints." *Journal of Materials Physics and Chemistry* 1, no. 4 (2013): 65-68. doi: 10.12691/jmpc-1-4-2.

1. Introduction

Stainless steels are used in several applications such as energy generation systems, heat exchangers and automotive, oil and chemistry industries [1,2]. Austenitic stainless steels (ASS) have high toughness, low machinability and the best resistance to scale formation among the stainless steel family. In addition, ASS have higher corrosion resistance than martensitic and ferritic stainless steels (FSS). In the other hand, FSS have higher resistance to chloride stress corrosion cracking and represent an economic option than ASS [3]. In addition, FSS have higher thermal conductivity and lower thermal expansion coefficient than ASS [4].

Some applications require joining ASS and FSS [5], which has been carefully studied because of the low weldability of FSS and the hot corrosion cracking of ASS [3,4,6]. Controlling the solidification and reached temperatures during welding becomes critical and represents an engineering challenge, since many of the precipitates present in the austenitic parent metal can be dissolved during the welding due to the high temperatures reached during the process (near to the solidus temperature). This generates an oversaturation of the austenitic matrix upon cooling, which may lead to the formation of precipitates in the heat-affected zone (HAZ). Such precipitates are mainly chromium carbides and chromium nitrides (M23C6 and Cr2N) that can decrease the corrosion resistance leading to intergranular corrosion [7].

This research studies the microestructural evolution of dissimilar austenitic (AISI 316L)-ferritic (AISI 430) stainless steels weldings using two different electrodes: austenitic AWS E309L and duplex AWS E2209-16 and varying the heat input in a low range (0.7-1.0 J/mm).

2. Experimental Procedure

SMAW welding was performed on "V" notched AISI 430 FSS and AISI 316L ASS parent metals with dimensions 200 mm x 100 mm and 4 mm thick. Welding was accomplished using two different electrodes (3.2 mm diameter): austenitic AWS E309L and duplex AWS E2209-16. The joining was made with a single pass welding and keeping a low heat input (HI), 0.8-1.0 kJ/mm for the austenitic electrode and 0.7-0.8 kJ/mm for the duplex electrode. The parameters used to control the heat input were current (I), voltage (V) and welding speed (v) (see Table 1). Chemistry of the parent metals was determined by optical emission spectroscopy (OES). Chemistry of the filler material was obtained from the provider data sheet (Table 2). The same welder made all welds in flat position.

Table 1. Heat input welding parameters

Electrode	v (mm/s)	I (A)	V (V)	HI (J/mm)	HI average
AWS E309L	1.9	50	49.0	1000	922 ± 79
	2.5	52	50.0	842	
	2.3	52	50.4	924	
AWS E2205-16	2.7	50	48.8	731	754 ± 40
	2.7	50	48.8	731	
	2.4	50	48.8	800	

Microstructure analysis was performed in the welded metals and the heat affected zones (HAZ) of the samples

in both sides (FSS and ASS). Samples were prepared using standard metallographic techniques with a 0.03µm alumina final polish. Etching was accomplished using aqua regia.

Tensile test was performed according to ASTM E8 [8]. Tensile specimens were 2 mm thick. Delta (δ) ferrite measurements were accomplished using a ferritoscope (Fischer MP30E S). Vickers microhardness profiles were obtained using 500 g load for 15 s. All measurements were performed perpendicular to the welding direction.

Table 2. Chemistry of parent metals and electrodes

Stainless steel	C (%w)	Cr (%w)	Ni (%w)	Si (%w)	Mn (%w)
AISI 430	0.030	16.660	0.147	0.491	0.345
AISI 316L	0.011	16.838	9.998	0.558	1.348
E309L	0.030	23.700	13.700	0.800	0.850
E2209-16	0.026	22.800	9.300	0.730	0.680
Stainless steel	Cu (%w)	Ti (%w)	Mo (%w)	P (%w)	N (%w)
AISI 430	0.103	0.013	-	0.025	-
AISI 316L	0.104	0.011	2.021	0.039	-
E309L	0.060	-	0.040	0.030	-
E2209-16	0.110	-	3.100	0.020	0.200

3. Results and Discussion

3.1. Microstructural Characterization

Figure 1 and Figure 2 show the microstructure profiles of the welded joints obtained with austenitic (AWS-E309L) and duplex (AWS-E2209-16) filler metals, respectively. There was a difference in size of the HAZ on the ferritic side (HAZ-F), which was larger for the austenitic electrode (~2 mm) than for the duplex electrode (~1.5 mm), which may be attributed to the differences in the heat input. In both cases, the HAZ on the austenitic side (HAZ-A) showed the absence of grain growth, the presence of equiaxial austenitic grains with twins and precipitates at the grain boundaries (Figure 3), this precipitation commonly occurs between 425°C y 800°C [6,7]. In addition, the fusion boundary (FB) next to the austenitic parent metal (ABM) has a partially melted zone with equiaxial austenitic grains and δ ferrite dendrites in the austenitic grain boundaries (Figure 4).

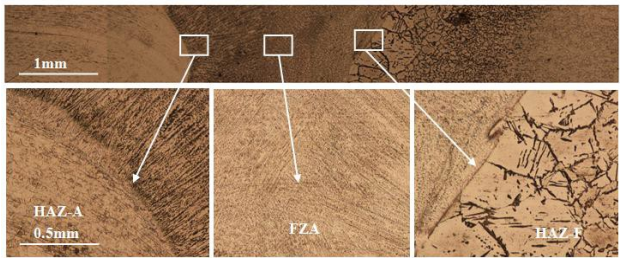

Figure 1. SMAW welding AISI 316L-AWS E309L-AISI 430

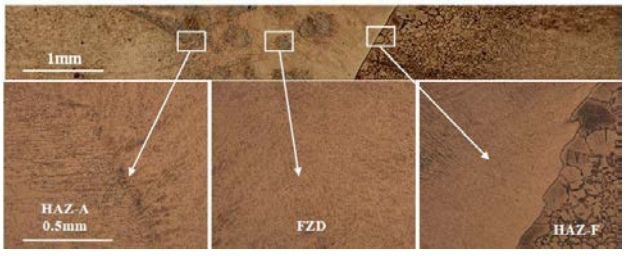

Figure 2. SMAW welding AISI 316L-AWS E2209-16-AISI 430

The microstructure of the fusion zones (FZ) depended on the composition of the filler metal. Austenitic stainless steel weld metal provided a microstructure in the FZ consisting on an austenitic matrix (white) with skeletal or vermicular ferrite -dark etching- (Figure 5a), this microstructure is obtained when weld cooling rates are moderate and/or when Creq/Nieq is low but still within the ferrite-austenite (FA) range. The FA solidification mode starts with primary ferrite solidification followed by the formation of austenite along the ferrite cell and the dendrite boundaries. As the weld metal cools the ferrite becomes increasingly unstable and the austenite begins to consume the ferrite by a diffusion-controlled reaction, [7]. The skeletal morphology is a consequence of the advance of the austenite consuming the ferrite. As the process proceeds, the ferrite is enriched in ferrite promoting-elements and depleted in austenite promoting elements, which makes it stable at lower temperatures where diffusion is limited.

Duplex stainless steel weld metal solidified as columnar ferrite grains perpendicular to the plate surface with fine acicular austenite at the grain boundaries (Figure 5b). High Creq/Nieq ratios lead to Type F solidification, i.e., ferrite is the only phase that forms directly from the liquid. Ferrite to austenite transformation subsequently occurs in the solid state, at temperature between 1300°C and 800 °C. In the weld metal, ferritic solidification involves an epitaxial growth from parent material at the fusion boundary. The epitaxial and competitive nature of ferrite grain growth in duplex stainless steel welds promotes the formation of a coarse columnar ferrite grain structure. The austenite starts to precipitate at the ferrite grain boundaries and at the weld metal surface due to higher free energy of these locations. The morphology of austenite, such as Widmanstätten side plates or intragranular plates, is dependent on the ferrite grain size and cooling rate [7,9].

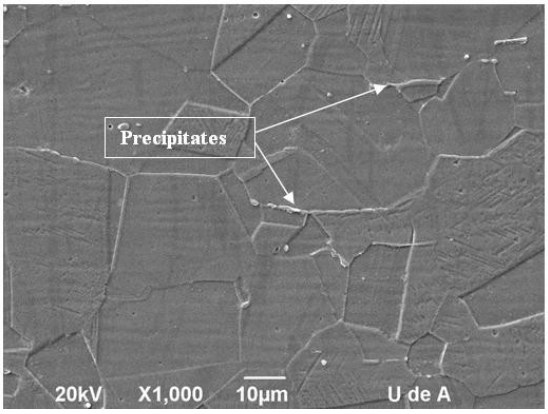

Figure 3. Heat affected zone on the austenitic side showing precipitates at the grain boundaries

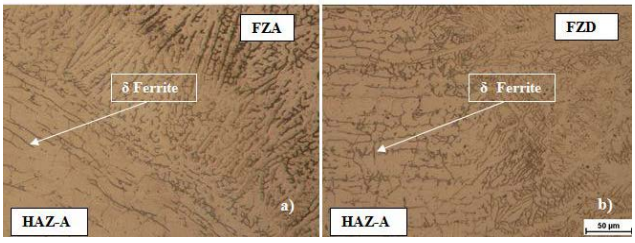

Figure 4. Fusion boundary microstructure a) AISI 316L-AWS E309L y b) AISI 316L-AWS E2209-16

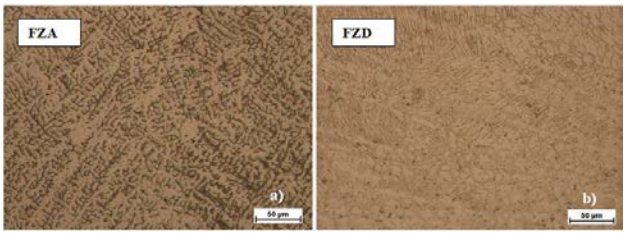

Figure 5. Microstructure of FZ a) AWS 309L y b) AWS 2209-16

The following microstructural features were the same for both filler metals: the fusion boundary next to the ferritic parent metal (FB-F) showed a columnar solidification growing from the ferrite parent grains (Figure 6). A coarse grain zone follows by a refined grain zone are observed in the HAZ-F and martensite was formed at the ferrite grain boundaries in all HAZ-F (see Figure 1, Figure 2, Figure 7). The coarse grain zone is formed because grain growth is diffusion controlled, driven by surface energy and requires no nucleation, the energy is given by the welding process [10]. The refined grains zone is due to a recrystallization process where new grains are formed by the movement an annihilation of dislocations in the grains previously deformed in the parent metal [7,11]. Regarding martensite formation, any austenite that forms at elevated temperature will transform to martensite upon cooling to room temperature leaving no carbon available for carbide formation, this happens preferentially at the grain boundaries (see Figure 8) [7].

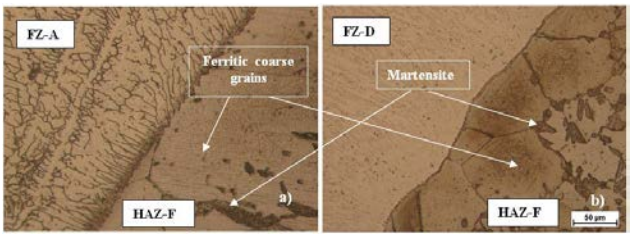

Figure 6. Microstructure of FB a) AISI 430-AWS E309L y b) AISI 430-AWS E2209-16

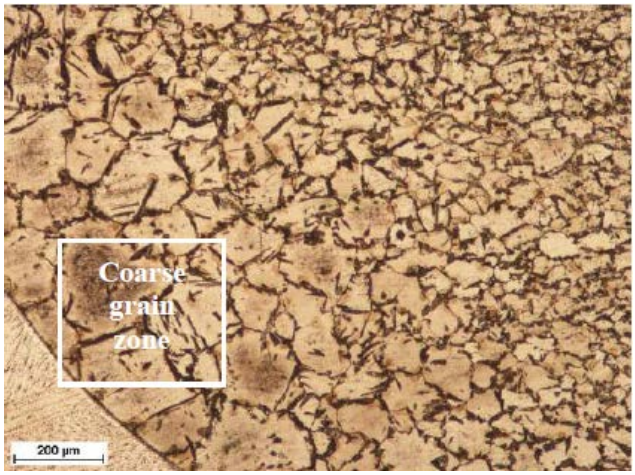

Figure 7. Microstructure of HAZ-F of AISI 430-AWS E309L

The austenitic filler metal generates a larger grain growth (264 µm mean grain size) than the duplex filler metal (156 µm mean grain size). This can be explained because of the heat input of the two experimental conditions, which was higher for the austenitic filler metal (see Table 2). In addition, duplex filler metal may produce higher cooling rates and lower reached temperatures than austenitic filler metal because of the differences in thermal properties.

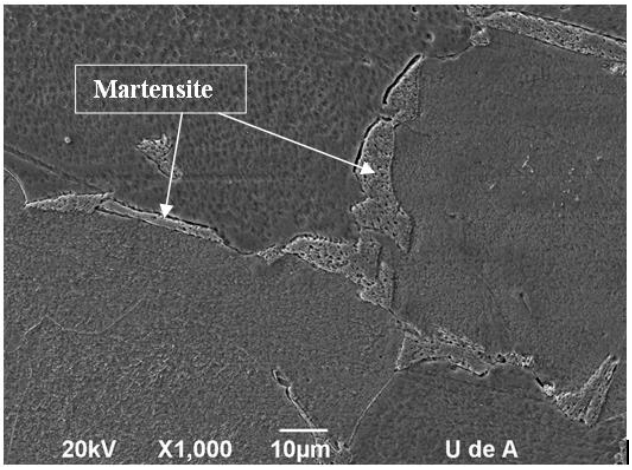

Figure 8. HAZ-F showing grain boundaries free of precipitates

3.2. Tensile Properties

The tensile behavior of the welded joints was similar for both experimental conditions (Table 3). Failure occurs at the ferritic parent metal and far away from the HAZ with ductile fracture. These results indicated that grain growth and martensite formation on HAZ-F were not decisive factors in the failure of the tensile probe. Figure 9 shows stress in function of strain.

Table. 3 Tensile properties

Filler metal	Tensile strength (MPa)	Yield strength (MPa)	Elongation (%)
AWS E309L	485	378	34
AWS E2209-16	505	361	36

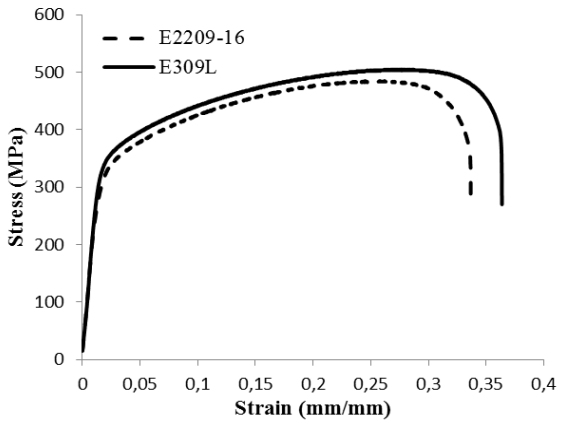

Figure 9. Stress vs strain curves of the welded joints

3.3. Microhardness and Amount of Delta Ferrite

Microhardness profiles were taken along a line in the middle of the thickness and included the parent metals, HAZ and FZ (Figure 10). In Figure 8, ¨0¨ indicates the center of the fusion zone. The main hardness differences are in the FZ and in the coarse grain zone of the HAZ-F, which was expected because of the difference in the amount and morphology of delta ferrite for each filler metal [12] and the

difference between the coarse ferritic grain sizes in the HAZ-F zones. The average hardness of the austenitic and duplex filler metals were 228 HV and 278 HV respectively.

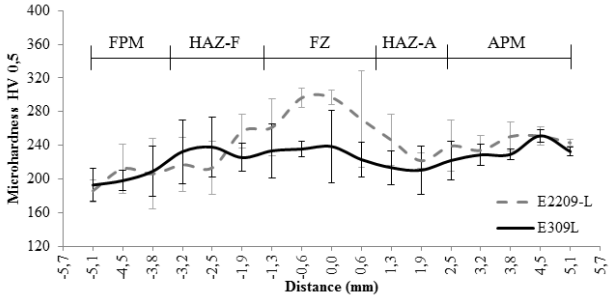

Figure 10. Microhardness profiles of the coupons

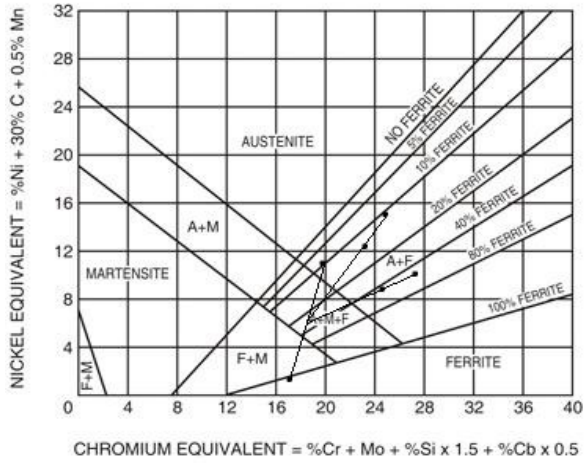

Figure 11. Schaeffler diagram

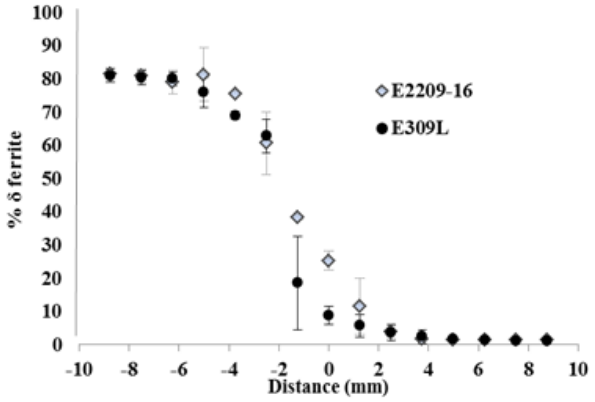

Figure 12. Delta ferrite profiles of the coupons

Shaeffler's diagram was used to predict the delta ferrite percent using 30% dilution. The results were 14% and 43% of delta ferrite for the austenitic and the duplex filler metals, respectively (see Figure 11). Delta ferrite was also measured using a ferritoscope, which indicated that delta ferrite were 9% for the austenitic electrode and 27% for the duplex filler metal (see Figure 12). The differences between the predicted and measured delta ferrite may be explained by: (1) Shaeffler's diagram does not take into account nitrogen to calculate the equivalent nickel [6,7], and (2) the real dilution may have been different than 30% used for the prediction [13].

4. Summary

The microstructural evolution of a dissimilar austenite-ferrite stainless steel welding was studied using two different filler metals and small variations in the heat input. The results indicated the size of the HAZ-F and the average size of the ferrite in the coarse grain zone depended on the heat input. In the other hand, the morphology and amount of delta ferrite is a function of the chemical composition of the filler metal.

Acknowledgement

The authors would like to acknowledge the financial support from the University of Antioquia, CODI, researching project MDC 01-7-10 and the financial support from COLCIENCIAS through the Young Researcher Scholarship Program. And acknowledge XIII Congress of Science and Technology of Metallurgy and Materials, Iguazú, Argentina, August 20-25, 2013.

References

[1] Khan, M.M.A., Romolia, L., Fiaschib, M., Dinia, G. and Sarri F., "Laser beam welding of dissimilar stainless steels in a fillet joint configuration", Journal of Materials Processing Technology, 28. 856-867. Nov. 2011.

[2] Celik, A. and Alsaran, A., "Mechanical and Structural Properties of Similar and Dissimilar Steel Joints", Materials Characterization, 43. 311-318. July 1999.

[3] Lakshminarayanan, A.K., "Effect of Welding Processes on Tensile and Impact Properties, Hardness and Microstructure of AISI 409M Ferritic Stainless Joints Fabricated by Duplex Stainless Steel Filler Metal", Journal of Iron and Steel Research, International, 16. 66-72. April 2009.

[4] Rajaković-Ognjanović, V., "Corrosion of an austenite and ferrite stainless steel weld", Journal of the Serbian Chemical Society, 76. 1027-1035. Dec. 2011.

[5] Reddy, G. M., Rao, K. S. and Sekhar, T., "Microstructure and pitting corrosion of similar and dissimilar stainless steel welds" *Science and Technology of Welding and Joining*, 13 (4). 363-377. Jan. 2008.

[6] Folkhard, E. *Welding Metallurgy of Stainless Steels*; Springer-Verlag Wien, New York, 1996.

[7] Lippold, J. and Kotecki, D., *Welding metallurgy and weldability of stainless steel*, John Wiley and Sons, USA, 2005.

[8] ASTM E8 - 13a Standard Test Methods for Tension Testing of Metallic Materials. ASTM International.

[9] Kaçar, R., "Effect of solidification mode and morphology of microstructure on the hydrogen content of duplex stainless steel weld metal", *Materials and Design*, 25. 1–9. Aug. 2003.

[10] Easterling, K., *Introduction to the physical metallurgy of welding*, Butterworks Monographs in Materials, UK, 1983.

[11] Granjon, H., *Fundamentals of welding metallurgy*, Woodhead Publishing Ltd, UK, 1991, 123-130.

[12] Duarte, P., "Mechanical and Microstrutural Characterization of Weldments of Ferritic Stainless Steel AISI 444 Using Austenitic Stainless Steels Filler Metals". *Journal of ASTM International*, 9 (2). 1-9. Jan. 2012.

[13] Kaçar, R., "An investigation of microstructure/property relationships in dissimilar welds between martensitic and austenitic stainless steels" *Materials and design*, 25. 317-329. Oct. 2003.